ADVANCED MATERIALS TECHNOLOGIES
www.advmattechnol.de

A Breathable and Stretchable Metastructure for a Versatile Hybrid Electronic Skin Patch with Long-Term Skin Comfort

Wonseop Hwang, Juhee Kim, Seongjin Park, Tae-Hyung Kang, Sunho Kim, Kijung Lee, Myoung-Gyu Lee, Rhokyun Kwak, In-Suk Choi, and Hyunjung Yi**

With increasingly diverse functionalities of electronic skins (E-skins), components and structures for the E-skin have also become more diverse and complex. It is extremely challenging to make all the components and devices required for additional functionalities stretchable and breathable to ensure skin comfort. Herein, we report a facile strategy to realize a versatile hybrid E-skin patch with great skin comfort by developing a breathable and stretchable metastructure to serve as the platform material of the hybrid E-skin patch. A Kagome-based mechanical metastructure made of breathable, stretchable medical adhesive integrates and tethers non-stretchable or stiff components and devices to the skin, allowing for both the breathability and mechanical comfort of skin. A wireless skin sensor system to sense electrocardiogram (ECG) signals and wirelessly transmit ECG signals in an event-driven manner such as sending R peaks only is developed on a polyimide-based flexible printed circuit board. The Kagome metastructure-tethered wireless ECG sensor patch does not cause significant skin discomfort when worn for five days, and successfully enables the event-driven wireless monitoring of ECG signals. We envision that this facile and versatile approach expands the type of materials and functionalities of E-skin for digital healthcare, personalized medicine, and smart prosthetics with emerging functionalities.

1. Introduction

On-skin electronic devices[1–6] that can detect bio-signals and convert them to electrical signals have attracted increasing interest over the last decade in the fields of digital healthcare,[7,8] personalized medicine,[9] neuro-engineering,[10] human-machine interfaces,[11,12] and smart prosthetics.[13] Monitoring of bio-signals by electrical means enables an integration of the electronic skin (E-skin) sensor with big data,[14] artificial intelligence,[15] and internet of things (IoT) technologies.[16] As the applications of on-skin devices expand, novel approaches to realize wearable electronics on non-conventional substrates such as 3D freeform surfaces, skin, and topographic substrates have been reported.[8,17,18] Moreover, additional attractive functionalities of E-skin have been also demonstrated. For example, implementing optical functionality to visualize information related to health conditions is an attractive direction in terms of intuitive interaction with humans.[19] Wearable sensors with self-powering functionality can also extend their applicability.[20,21]A wireless E-skin system that transmits the measured data to mobile devices and enables daily activities while monitoring health conditions is also attractive in terms of user convenience.[22] Moreover, the possible functionality to transmit only key necessary information out of the bio-signals is a particularly attractive direction for the E-skin sensor in that it can reduce the power consumption for wireless data transmission and the number of data for post-processing.

W. Hwang, S. Park, T.-H. Kang, S. Kim, H. Yi
Post-Silicon Semiconductor Institute
Korea Institute of Science and Technology
Seoul 02792, Republic of Korea
E-mail: hjungyi@kist.re.kr

J. Kim, K. Lee, M.-G. Lee, I.-S. Choi
Department of Materials Science and Engineering
Seoul National University
Seoul 08826, Republic of Korea
E-mail: insukchoi@snu.ac.kr

The ORCID identification number(s) for the author(s) of this article can be found under https://doi.org/10.1002/admt.202200477.

© 2022 The Authors. Advanced Materials Technologies published by Wiley-VCH GmbH. This is an open access article under the terms of the Creative Commons Attribution-NonCommercial-NoDerivs License, which permits use and distribution in any medium, provided the original work is properly cited, the use is non-commercial and no modifications or adaptations are made.

DOI: 10.1002/admt.202200477

R. Kwak
Department of Mechanical Convergence Engineering
Hanyang University
Seoul 04763, Republic of Korea

M.-G. Lee, I.-S. Choi
Department of Materials Science and Engineering
Research Institute of Advanced Materials (RIAM)
Seoul National University
Seoul 08826, Republic of Korea

H. Yi
Department of Materials Science and Engineering
YU-KIST Institute
Yonsei University
Seoul 03722, Republic of Korea

Many of these functionalities inevitably require additional functional components and devices in addition to the sensing electrodes and devices. For example, a wireless E-skin sensor system usually consists of several functional components—such as analog circuits and filters as well as a wireless microcontroller unit (MCU) including an analog-to-digital converter (ADC) and Bluetooth low energy (BLE) interface for wireless communication. Moreover, to realize event-driven monitoring of biosignals requires an appropriate algorithm and relevant hardware within the E-skin. A battery unit is also necessary to operate the E-skin system. Employing commercially available components within the E-skin can provide a facile and reliable approach to implement additional functionalities to E-skin. However, the commercially available components and systems are usually non-stretchable or rigid and thus can cause significant skin discomfort if directly attached to the skin. In general, it is extremely challenging to make all of the system components and batteries ultrathin and/or stretchable so that they are mechanically compliant with the skin for skin-comfortable E-skin. Therefore, an approach to enable integration of skin-incompatible components with E-skin and to ensure great skin comfort of such hybrid E-skin is highly necessary. Several approaches to decouple the sensor system based on rigid/non-stretchable components from the skin have been proposed.[6,22] For example, a decoupling chamber made of a soft elastomeric material or an ionic liquid layer was inserted between the skin-interfacing sensing electrode and the circuits to fabricate skin comfortable hybrid E-skin. However, these approaches either require complex processes or can potentially suffer from leakage.

Mechanical metamaterials are carefully structured materials that display exotic properties such as negative Poisson's ratio and stiffness modulation and often consist of periodically arranged building blocks.[23,24] Auxetic structures, a type of mechanical metamaterial, have been widely used for flexible and stretchable devices.[25–30] In particular, 3D and 2D soft network structures with rational design strategy have been shown to closely match the non-linear stress-strain responses of biological tissues.[31–35] By arranging the building blocks of auxetic structures carefully, not only the mechanical properties but also their breathability can be greatly improved due to their intentionally designed open structures. For example, porous auxetic structures and auxetic kirigami structures have been reported to enable sweat-permeable E-skin.[28,36] Therefore, a carefully designed auxetic structure could provide a skin comfortable E-skin platform structure that addresses both the mechanical and breathable aspects of skin. However, previous reports focused on the homogeneous contact type of the E-Skin, that is, conformal contact with the skin. So far, a metastructure-based approach to address the heterogeneous contact requirements of the hybrid E-skin patch, that is, the conformal contact of the sensing electrode with the skin and mechanical decoupling of the sensor system consisting of rigid and non-stretchable components and devices from the skin has been elusive.

Herein, we report a facile approach based on a mechanical metastructure to realize a versatile hybrid E-skin patch with long-term skin comfort by developing a breathable and stretchable metastructure and introducing a tethering scheme to the metastructure. We designed the mechanical metastructure based on skin strain distributions under various body motions, and stretchability, porosity, and the geometrical parameters of the hybrid E-skin sensor patch. As a demonstration of a versatile hybrid E-skin patch that operated for a long time with great skin comfort, a wireless all-in-one electrocardiogram (ECG) sensor system was developed based on a flexible printed circuit board (FPCB) and tethered to the skin via the Kagome metastructure. An algorithm to enable the detection of R peaks of ECG signals and event-driven wireless transmission of R peaks was also developed and implemented in the sensor system. Trials with human participants demonstrated that the Kagome metastructure-tethered wireless ECG sensor patch did not cause noticeable skin discomfort for five days and successfully enabled the event-driven wireless monitoring of ECG signals. This facile strategy provides a new opportunity to expand the types of materials and components for the development of emerging on-skin devices and sensors with versatile functionalities.

2. Results and Discussion

2.1. Overview of a Breathable, Stretchable Metastructure-Based Hybrid E-skin Patch

A schematic layout of the hybrid E-skin patch based on a breathable and stretchable metastructure is presented in **Figure 1**a. The hybrid E-skin patch consisted of three layers: a top Kagome metastructure layer made of a breathable, stretchable biomedical adhesive with its adherent surface on its bottom side, a polyimide (PI)-based wireless sensor system, and a bottom layer with a partial Kagome metastructure made of the same breathable, stretchable biomedical adhesive with its adherent surface on its upper side to attach the sensor system to the top Kagome layer. The top Kagome metastructure layer provided a structural platform material of the sensor patch. As the base material of the sensor patch platform, we used a commercially available breathable, stretchable biomedical adhesive—namely Tegaderm (3M), a polyurethane-based elastomeric film with an adherent layer on one side. Tegaderm has been widely used because of its high breathability and its conformable attachment to the skin.[37] Since skin is an open system in that there is a continuous diffusion of water vapor through the skin, blocking the surface of skin can cause discomfort and cause the skin to be afflicted with irritation and stuffness and to be potentially prone to developing rashed and inflammation when the breathability of the skin impeded for a long time.[38–42] The water vapor transmission rate (WVTR) of the Tegaderm was measured to be 14.47 ± 0.30 g/m^2/h (Supplementary Methods and Figure S1), a value higher than the WVTR of normal skin (8.5 ± 0.5 g/m^2/h).[42] The Kagome metastructure was systematically designed to be comfortable on the skin and to yield a stable device by considering the skin strain distribution and stress under various motions. The Kagome metastructure also significantly increased the WVTR of the sensor patch (Supplementray Figure S1). A detailed description of the design procedure is provided in the next section below.

Regarding the sensor system, of the various biosignals, the ECG signal was chosen in this study based on its importance for long-term monitoring for personalized and preventive healthcare. An ECG sensor system with FPCB-based dry sensing electrodes is illustrated as an example of a wireless

© 2022 The Authors. Advanced Materials Technologies published by Wiley-VCH GmbH

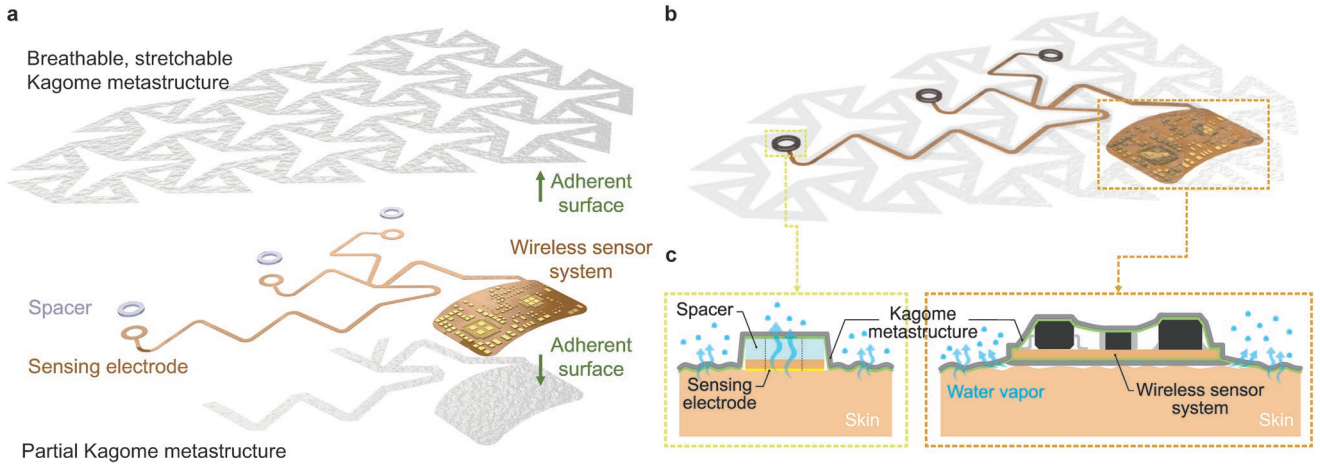

Figure 1. Overview and structures of the breathable, stretchable Kagome metastructure-based hybrid E-skin sensor patch. a) A layer-by-layer schematic layout of the Kagome metastructure-tethered wireless ECG skin sensor patch. Both the top and bottom layers were fabricated using the breathable biomedical dressing film, Tegaderm. b) Schematic of the assembled hybrid E-skin patch. c) Schematic of the cross-sectional view of the skin-tethered hybrid E-skin sensor patch via the metastructure. The adhesive sides of the bottom and top layers are indicated as green. The FPCB-based wireless sensor system was not directly attached to the skin but tethered to the skin through the breathable Kagome metastructure. This scheme based on tethering allowed for both the breathability and comfort of the skin even in the presence of the non-breathable and non-stretchable FPCB.

sensor system. The bottom layer of the sensor patch was designed to cover the circuit system and the interconnections but not the sensing electrodes and then attached to the all-in-one ECG sensor system as illustrated in Figure 1a–c. Therefore, the assembled hybrid sensor patch was directly attached to the skin only through the areas not containing the circuits and interconnection lines—that is by using a scheme involving tethering. This tethering also allowed for the excellent breathability of the wireless sensor patch; the breathable sensor patch platform material, namely Tegaderm, was permeable to water vapor, and water vapor molecules underneath the circuit and the interconnections were able to diffuse through the free space formed by the tethered structure as illustrated in Figure 1c. Therefore, the hybrid E-skin patch tethered to the skin via the breathable and stretchable metastructure enabled direct contact of the sensing electrodes with the skin and yet provided both breathability and mechanical comfort to the skin underneath the non-breathable and non-stretchable sensor system.

2.2. Design of the Mechanical Metastructure for the Hybrid E-skin Patch Platform

To systematically design the platform structure of the hybrid E-skin patch, the skin strain levels were analyzed using the digital image correlation (DIC) method, which is a non-contact-type full-field strain measurement method.[43] Here, a chest area was examined because the chest area is a challenging location for E-skin applications due to its complex skin strain and stress distributions during daily activities and also can be used for ECG monitoring. The size and location of the analyzed area were determined based on the locations of the ECG electrodes (Supplementary Figure S2 and S3) and the size of the wireless sensor system as discussed below. The location of the analyzed area (having dimensions of 10 cm × 12 cm) around the chest is indicated as boxes in **Figure 2**a and Supplementary Figure S4. The skin strain distribution of the chest was measured under two representative motions that induced a large extension: raising of the arm upward (Motion 1) and to the side (Motion 2). The left and middle panels of Figure 2a show the strain levels of bare skin subjected to Motion 1 (left panel) and Motion 2 (middle panel). The white arrows indicate the stretching direction of the maximum principal strain. In the case of Motion 1, the lower part of the diagonal stretched along the vertical direction, whereas the upper part of the diagonal stretched along the direction inclined at 30° with respect to the vertical direction. While the strain levels during both Motion 1 and Motion 2 increased as the area approached the bust point, the skin deformed to a greater extent during Motion 1, and the maximum local strain was near 30% at the uppermost area where the patch would be attached. Therefore, it is highly desirable for the stretchability of the sensor patch to be isotropic and to accommodate deformations along with various directions.

The skin strain distribution was further examined after attaching a rectangular Tegaderm film to the chest skin area and the DIC analysis result is shown in the right panel of Figure 2a. The strain was observed to be concentrated along the edges of the patch, reaching a maximum strain level of higher than 30% and thus causing considerable stress and severe discomfort in the skin. This result was ascribed to the large difference between the elastic modulus of the skin[35,44,45] and that of the Tegaderm film (~9 MPa) (Supplementary Methods and Figure S5–S7). Therefore, it was crucial to design a patch structure having an effective elastic modulus comparable to that of the skin in order to decrease the strain at the edges of the patch and hence make the patch more comfortable on the skin.

Of the diverse auxetic structures found in a literature search (Supplementary Methods and Figure S8), the re-entrant, rotating squares, lozenge grid, and Kagome structures were selected as the candidate skin patch structures based on the simultaneous requirement of stretchability, porosity, and geometrical parameters for ECG sensing applications such as the

© 2022 The Authors. Advanced Materials Technologies published by Wiley-VCH GmbH

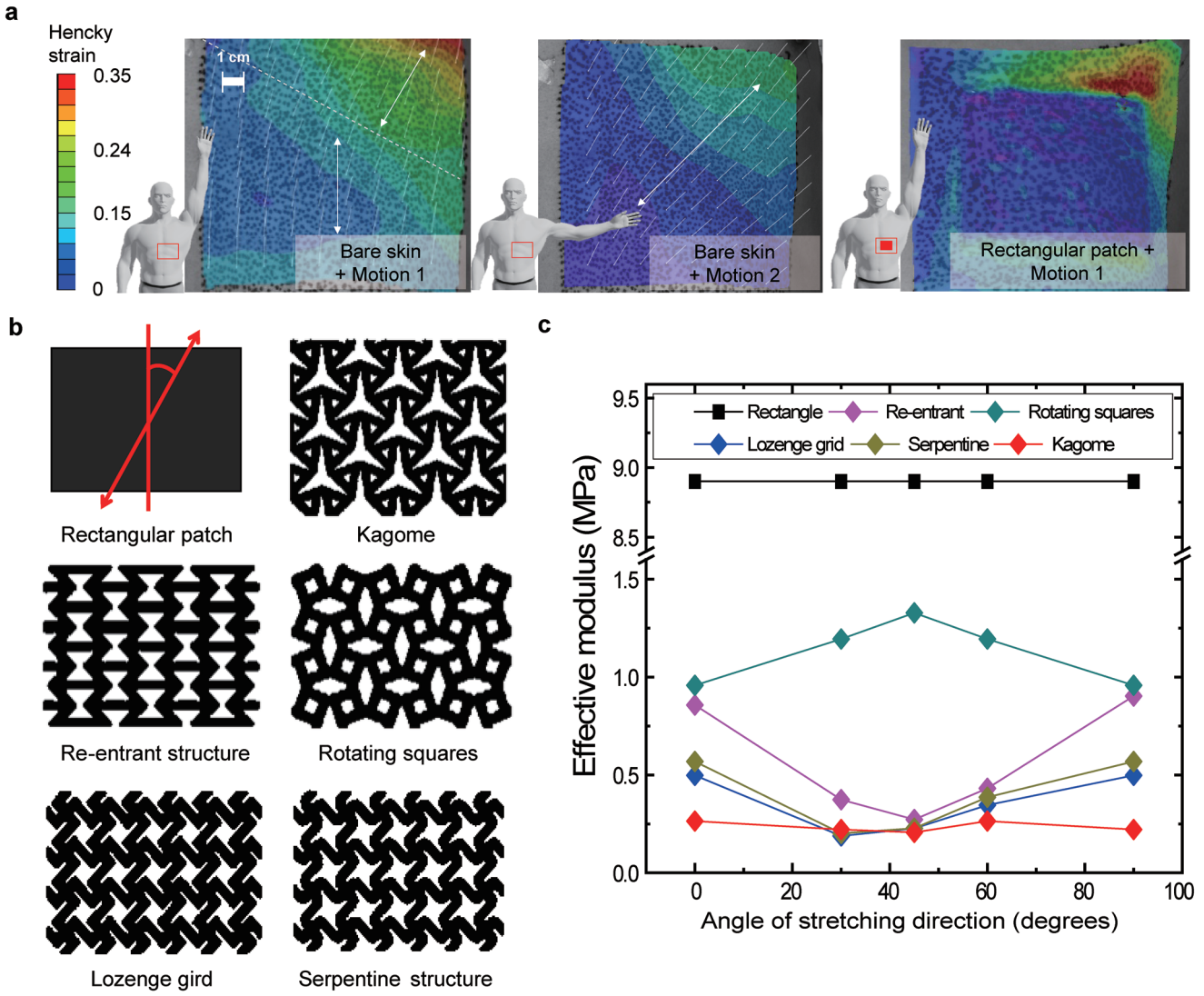

Figure 2. Design of the mechanical metastructure for the hybrid E-skin patch platform. a) Skin strain distributions of the chest under various arm motions with and without an attached rectangular patch of the Tegaderm breathable medical dressing. b) Various designs of different mechanical metastructures for the skin patch platform, with the rectangular structure being a control structure. c) Calculated effective moduli of various mechanical metastructures shown in panel (b) as a function of stretching direction.

electrode size, spacing, interconnect arrangements, and circuit design. A serpentine pattern was included for comparison because it is a commonly used structure for wearable sensors. Geometrically, these structures can stretch by more than 30%, comparable to the maximum local strain of the skin in the area around the attached patch. To ensure both a stretchability of >30% and porosity of 50% of the chest patch, the hinge angles and the voids inside the structure were carefully designed. A detailed description of this design strategy is provided in the Supplementary Methods and Figure S9. The final various designs of different mechanical metastructures are shown in Figure 2b.

The capability of each structure to accommodate stretching deformations in various directions was investigated using finite element simulation. Here, an effective elastic modulus was used as a descriptor to compare and sceen the desirable metastructure and determined from the slope of the stress-strain curve of each structure (Supplementary Figure S10). The calculated effective elastic moduli of each structure along stretching angles of 0°, 30°, 45°, 60°, and 90° with respect to the vertical direction (indicated by the red solid line in Figure 2b) are plotted in Figure 2c. For a stretching angle of 0°, the effective elastic modulus followed the order of rotating square (0.96 MPa) > re-entrant (0.86 MPa) > serpentine (0.57 MPa) > lozenge (0.50 MPa) > Kagome (0.26 MPa). This result suggested that introducing an appropriate patterned structure into the Tegaderm base material with a modulus of ~9 MPa can systematically tune the effective elastic modulus, significantly decreasing it to a level comparable with that of skin (~0.1 MPa). Also, the Kagome structure showed a modulus that was not only nearly isotropic but also the lowest in most stretching directions, whereas the effective elastic moduli of the other auxetic structures differed for the

© 2022 The Authors. Advanced Materials Technologies published by Wiley-VCH GmbH

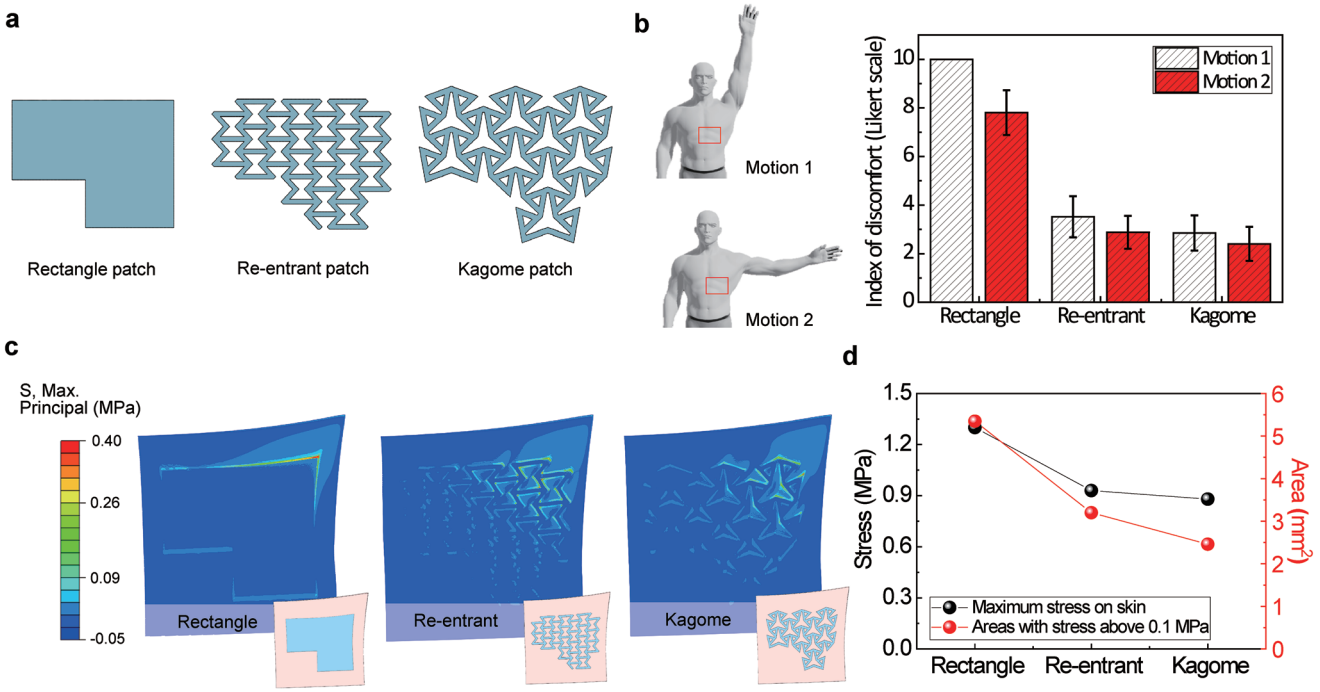

Figure 3. Design of the patch platform for the hybrid E-skin patch with skin comfort. a) Modified chest skin patch designs used for on-body evaluation of skin comfort and simulations. b) On-body evaluation result of the skin comfort of various patch designs shown in panel (a) under two different body motions. The index of skin discomfort was evaluated based on the Likert scale. c) Simulation results of the maximum principal stress contours of the chest skin after attaching the three patches shown in panel (a). d) Simulation results of the maximum skin stress and the size of the skin area showing a stress level higher than 0.1 MPa after attaching the patch structures shown in (a).

different directions. All of these results together suggested that, of the investigated designs, the Kagome structure would be the best in terms of skin comfort.

2.3. Design of the Patch Platform of the Hybrid E-skin Patch

The skin comfort levels of the developed mechanical metastructures to serve as the platform material for the hybrid E-skin patch were experimentally compared by carrying out a trial including human participants. For this trial, three structures were selected: the Kagome structure showed the lowest and most isotropic modulus; the re-entrant structure showed highly different moduli for different directions; the rectangular patch was used as a control. Here, the structures were slightly modified considering the application of the platform structure as the ECG patch while maintaining the mechanical properties and porosity of the previously designed patterns. First, the bottom-left part of each patch was removed as shown in **Figure 3**a to minimize the effect by breathing motions. Second, the rib width of the pattern was adjusted to be 3 mm to include an integer number of units and to place three electrodes spaced 3 cm apart from each other (Supplementary Figure S2) within a total area of 80 mm × 110 mm. Examples of the modified patch structures are shown in Figure 3a.

To quantify the skin comfort levels, a numerical rating scale or so-called the Likert scale method, a widely used pain rating method in the medical field, was utilized.[46,47] Because the level of discomfort is inevitably subjective to a certain extent, a human trial was performed by involving twenty-six participants and the results were statistically analyzed. Participants were asked to express the degree of skin discomfort from 0 (least uncomfortable) to 10 (most uncomfortable) while performing Motion 1 and Motion 2, respectively, with each patch attached. Figure 3b shows the results of the patch comfort test in which the skin comfort levels of the three patches were measured using the Likert scale method. According to ANOVA and F-test analysis, there was a significant difference in the mean of the index of discomfort between the three patches and between the two body motions as well. The mean indexes of the discomfort of the patches during Motion 1 (Motion 2) differed from one another at the significance level of 95% and were found to be 10 (7.8), 3.5 (2.9), and 2.8 (2.4) for, respectively, the rectangle, re-entrant, and Kagome structures, with this trend the same as that of the effective elastic modulus values. Thus, this result verified that, of the tested designs, the Kagome structure was the most suitable structure to use as a skin patch platform. Note that Motion 2 was more comfortable than Motion 1, presumably because the skin strain levels induced during Motion 2 were lower than those induced during Motion 1 and the moduli of the patterns when stretched along the diagonal direction were lower than those of the patterns when stretched along the vertical direction.

A finite element simulation was also conducted to explain the better comfort of the Kagome-structured patch on the skin in a numerical and objective manner. In particular, the stress level was chosen as the descriptor because the failure criteria in the mechanical behavior of material are typically based on

© 2022 The Authors. Advanced Materials Technologies published by Wiley-VCH GmbH

stress. The stress levels developed on the skin during the body motions were calculated while the patch-attached skin was deformed using the boundary conditions optimized based on DIC results (Supplementary Methods). The distributions of the calculated stress levels of the skin for the three different patches are presented in Figure 3c. The skin stress was largely localized around the edge of the skin sensor patch. The stress level increased upon proceeding upward along the diagonal direction, as was expected from the DIC analysis. The local maximum principal stress level of the skin decreased from 1.3 MPa for the rectangular patch to 0.93 MPa for the re-entrant one to 0.87 MPa for the Kagome one, as summarized in Figure 3d. That is, the maximum stress level for the Kagome-structured patch was lower than those of the rectangular and re-entrant-structured patches by 28% and 6%, respectively. Note that when the discomfort index for each structure for Motion 1 was normalized to 0~1, it appeared as Rectangular (1), Re-entrant (0.091), and Kagome (0) and this trend was similar to the normalized maximum principal stress value of Rectangular (1), Re-entrant (0.12), and Kagome (0). Also, the area of the region where the induced stress was higher than 0.1 MPa showed the same trend, i.e., with values of 5.4 mm^2, 3.2 mm^2, and 2.5 mm^2, for the rectangular, re-entrant, and Kagome structures, respectively. Therefore, the higher comfort afforded by the Kagome structure than by the rectangular and re-entrant structures can be explained by its reduced concentration of stress on the skin. The high correlation of the stress levels with the skin discomfort level is presumably ascribed to the J-shaped stress-strain response of the skin[1,35] because the non-linear behavior of skin at higher strains can cause adverse and irreversible effects[1] and in this region a small change in the strain level can produce a large change in stress levels. All these results suggest that comparing the maximum stress levels could help screen structures for skin comfortable E-skin patch.

2.4. On-Body Evaluations of Kagome Metastructure-Tethered Hybrid Wireless ECG Sensor Patch

As a demonstration of the Kagome metastructure as a promising platform material of a skin comfortable hybrid E-skin patch, a wireless chest skin sensor patch to detect the ECG signal and wirelessly transmit the measured ECG signals was developed as schematically illustrated in **Figure 4**a. An all-in-one ECG sensor system that included the dry ECG sensing electrodes and the circuit system in a single layer was fabricated using a polyimide (PI)-based commercial FPCB technology. The FPCB layer was designed to spatially segregate the sensing electrodes from the circuit system as shown in Figure 1a because of their different requirements for skin contact: the sensing electrode must make an intimate contact with the skin whereas the non-stretching FPCB-based sensor system should not be directly attached to the skin to ensure the mechanical comfort.

First, a circuit system for wireless sensing of ECG signals was developed. Figure 4b and 4c show the functional block diagram of the sensing system and the photograph of the fabricated system, respectively. The key functional components of the system were interfaces for the sensing electrodes, an instrumentation amplifier in an analog front-end (AFE) integration circuit (IC), low-voltage drop out (LDO) for power supply, analog filters (low-pass (LPF), high-pass (HPF), notch), and a microcontroller (MCU) with BLE. The functional block diagram depicts the signal truncation, filtering, processing, and wireless transmission. The cardiac electrical potential between the electrodes was differentially amplified by the instrumentation amplifier mounted in the AFE IC, and the analog output signal was passed through filters to remove noise. The improved analog signal was converted to data through the ADC of the MCU at a sampling rate of 200 Hz, and the converted data were transmitted to the user's smartphone through BLE communication.

The ECG sensing electrode was also fabricated using the FPCB technology to ensure both the long-term stability of the sensing electrode and its seamless integration with the sensing system, as illustrated in Figure 1a. The FPCB for the sensing electrode was designed as a ring shape to minimize the blocking of the skin surface by the non-breathable PI, and the copper (Cu) layer of the patterned FPCB was exposed and plated with electroless nickel immersion gold (ENIG) as shown in Figure 4d and Supplementary Figure S11. The surface of the dry electrode showed a rough morphology as presented in the scanning electron micrograph (Figure 4e). To enhance the contact quality of the dry electrode, a soft elastomeric spacer made of Ecoflex was used based on the analysis of the electrochemical impedance spectra (Supplementary Figure S12). The specific impedance levels of the dry electrode with the spacer were similar with those of the wet electrode in the low frequency range <~20 Hz which is relevant frequency range for the heart beat and QRS complexes (5~15 Hz)[48,49] whereas the dry electrode without the spacer exhibited a higher specific impedance, due to the poorer contact of the polyimide substrate of the Au electrode with the skin in the absence of the soft spacer. The wet electrode showed the least motion artifacts during severe body motions (Supplementary Figure S13), presumably due to the firm adhesion of the wet electrode enabled by the thick rigid metal electrode and the larger adhesive area. However, the firm adhesion of the wet electrode in turn produced a significant skin discomfort when attached for a long time. In summary, the developed Au dry electrode with the spacer enabled a low interfacial contact impedance and moderate motion artifacts that allowed for excellent sensing performance with long-term functionality and skin comfort as demonstrated below. A representative ECG signal acquired using the dry sensing electrode with the spacer clearly showed the characteristic P wave, QRS complex, and T wave as presented in Figure 4f.

The assembled final wireless hybrid ECG sensor patch is presented in Figure 4g. Before the on-body evaluation of the skin comfort of the Kagome metastructure-tethered hybrid E-skin patch, numerical simulations on the distributions of stresses on the skin and strains of the device after applying the Kagome metastructure-tethered hybrid wireless ECG sensor patch to the skin were performed and the results are presented in Figure 4h. The local maximum stress of the skin (left) was calculated to be 0.91 MPa—slightly increased, specifically by 4%, compared to the Kagome structure without FPCB but still lower than that of the re-entrant structure. More importantly, even though the FPCB material with a quite large elastic modulus (18 GPa) was applied to the sensor patch, skin comfort may not be reduced. In addition, to predict the sensor failure, the strain applied

© 2022 The Authors. Advanced Materials Technologies published by Wiley-VCH GmbH

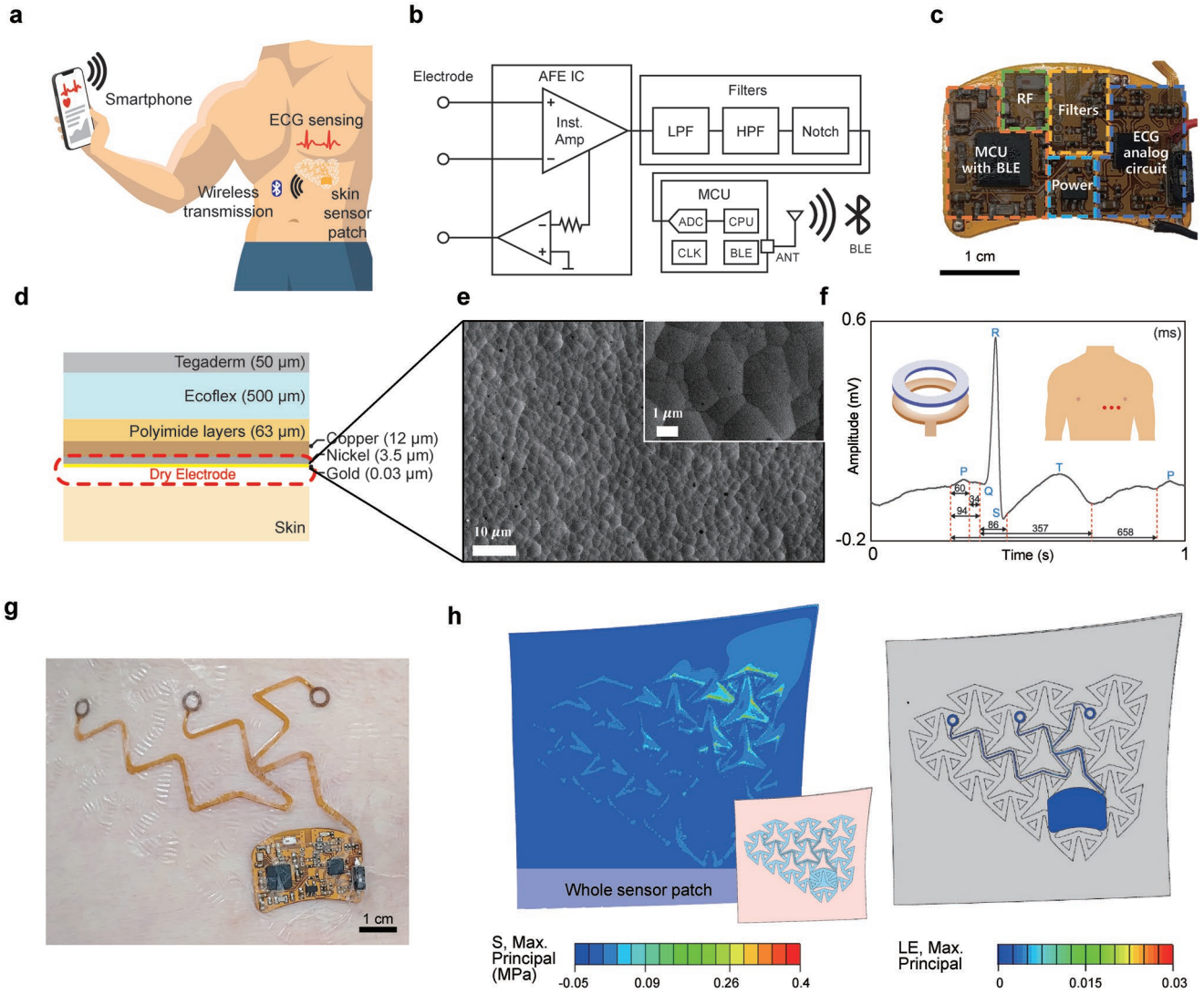

Figure 4. Kagome metastructure-tethered hybrid wireless ECG sensor patch with long-term functionality and skin comfort. a) Illustration of the wireless monitoring of ECG signals using a Kagome metastructure-tethered wireless sensor patch. b) Functional block diagram of the circuit system for wireless monitoring of ECG signals. The measured ECG signals through the dry electrodes were processed and wirelessly transmitted to the smartphone through BLE. c) Photograph of the fabricated circuit system with key components indicated. d) Schematic structure of the FPCB-based dry sensing electrode of the hybrid ECG sensor patch. e) Scanning electron micrograph of the dry sensing electrode based on the FPCB-based Au electrode (ENIG, electroless nickel immersion gold). f) A representative ECG curve acquired using the FPCB-based dry electrode with the soft spacer from the indicated locations on the chest as red dots. g) Photograph of the Kagome metastructure-tethered wireless ECG sensor patch attached to skin. h) Simulation results of the skin stress distribution and FPCB strain distribution with the Kagome metastructure-tethered wireless sensor patch on the skin.

to the FPCB was calculated and found to be less than 3%, far lower than the failure strain of the FPCB.[50–52] Therefore, the device was concluded to be mechanically stable and this sensor patch was concluded to be able to function sufficiently well under the conditions of stretching of the skin.

2.5. On-Body Evaluations of Kagome Metastructure-Tethered Hybrid Wireless ECG Sensor Patch

Next, human participant trials were performed with the Kagome metatstructure-tethered hybrid wireless ECG sensor patch. The sensor patch was attached to the rib area just below the left side of the chest and it was worn continuously and normal daily activities were performed such as studying, taking a shower, and sleeping as schematically illustrated in **Figure 5**a. A polymer battery was also connected to the sensor system (Figure 5b) and worn throughout the experiment for continuous on-body evaluation.

The ECG signals were measured for 2 minutes every hour over 20 h and the representative measured signals along with the enlarged ECG curves from several time points are shown in Figure 5c. The characteristic ECG signals were clearly monitored during various activities and even after taking a shower and sleeping. The signal-to-noise (SNR) levels of the ECG curves were also analyzed. The SNR of the ECG signal was very

© 2022 The Authors. Advanced Materials Technologies published by Wiley-VCH GmbH

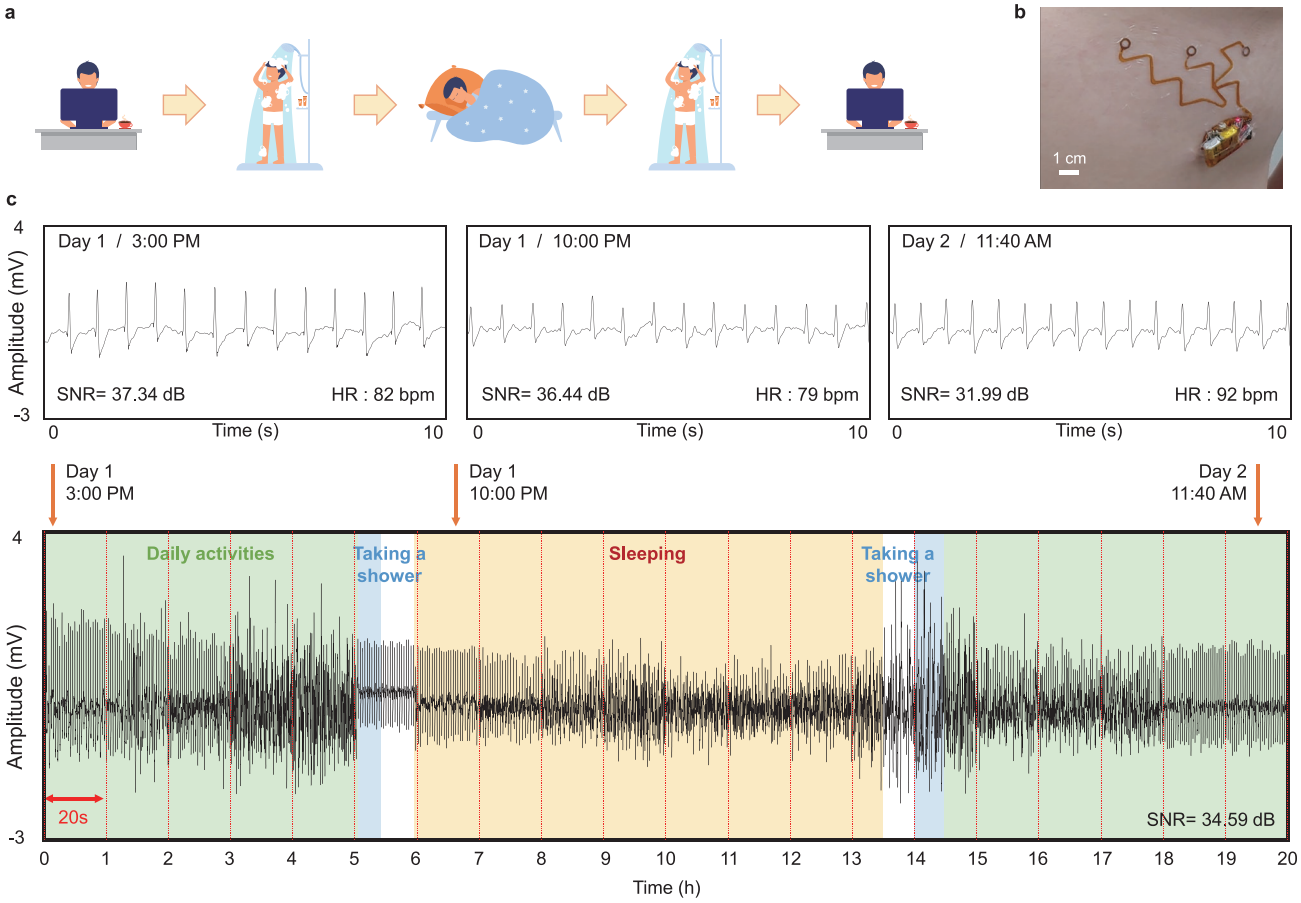

Figure 5. Continuous on-body evaluation of the hybrid wireless ECG sensor patch. a) Illustration of various daily activities performed during the on-body evaluation of the E-skin patch for 20 h. b) Photograph of the sensor patch on skin with a polymer battery connected to the sensor system. c) ECG signals measured during and after various daily activities including studying, taking a shower, and sleeping. The middle panels show enlarged ECG curves obtained from the several times indicated.

high >30 dB and the sensing performance slightly decreased only by 5.3 dB. More importantly, the average SNR of the comprehensive ECG signals acquired over 20 h was about 34.59 dB and this value was higher than the values reported in the literature using the state-of-art ECG E-skin systems (Table S1).[22,53,54] Note that the heart rate during sleeping was shown to be slightly lower than that during normal daily activities.

The skin comfort and the function of the sensor patch was further examined for extended time period. The sensor patch was attached for five days and ECG signals were measured once a day, at 2 PM for 2 minutes. Examples of the acquired ECG curves are shown in **Figure 6**a. No significant degradation in the sensing performance was observed with a slight decrease only by 3 dB for five days. This level of long-term stability of the sensor patch was comparable to the data reported in literature and the SNR level of 29.95 dB of ECG curves of Day 5 was also higher than the previously reported values using the-state-of-art ECG skin patches or hybrid electronics using gel electrolytes (Table S1).[22,54] Characteristics of ECG curves such as P wave, QRS complex, and T wave were clearly observed (Supplementary Figure S14), confirming the high quality of the acquired signals for clinical/medical settings. The clear characteristic waves of the ECG signals successfully demonstrated the capability of the sensor patch to wirelessly monitor ECG signals for at least five days.

Photographs of the Kagome metastructure-tethered hybrid wireless ECG sensor patch worn on the skin of a volunteer for one and five days, respectively, are shown in Figure 6b. Here, note the FPCB-based all-in-one wireless sensor system was clearly seen whereas the transparent Kagome patch platform was relatively difficult to see. Negligible skin irritation was observed during the attachment of the sensor for five days. Moreover, no significant irritation was also observed after it was then detached from the skin as shown in Figure 6b. This is in clear contrast to the case of a rectangular patch. When a rectangular-shaped Tegaderm patch was attached to the same chest skin area for 24 h, there were significant skin rashes and they lasted for longer than 48 h (Supplementary Figure S15). The skin abnormality induced by the commercially available, widely used biomedical dressing film is presumably due to the challenging nature of the chest area since the distributions of the skin strain and stress levels are complex and continuously changing during daily activities. All these results confirm the great potential of the Kagome metastructure-based approach for developing a hybrid E-skin patch with long-term functionality and skin comfort.

© 2022 The Authors. Advanced Materials Technologies published by Wiley-VCH GmbH

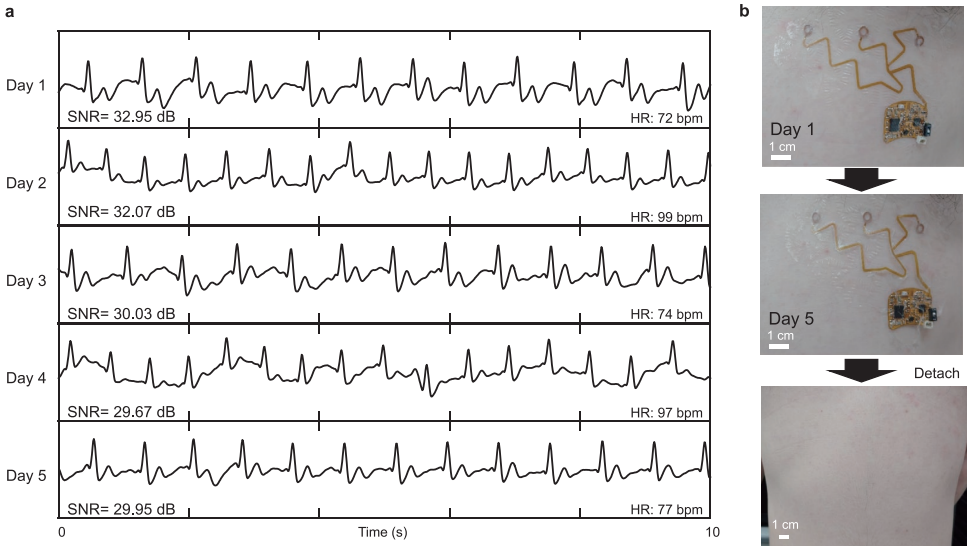

Figure 6. Long-term on-body evaluation of the hybrid wireless ECG sensor patch. a) Wireless readout of ECG signals when the sensor patch was worn for five consecutive days. ECG signals were measured at 2 PM every day for evaluating the long-term functionality of the patch. b) Photographs of the sensor patch continuously worn for one day (top) and five days (middle) and photograph of the skin immediately after detaching the sensor patch (bottom) attached to the skin.

These results also suggested that the use of the tethering-based scheme with the auxetic structure can expand the types of materials that can now be used to those that were previously excluded for the fabrication of skin sensor patches due to their high stiffness levels.

2.6. Facile Addition of Functionality of the Hybrid E-skin Patch

As a demonstration of an additive and versatile functionality of the hybrid E-skin patch, an algorithm to detect the R peak data and wirelessly send these data was developed and implemented in the MCU firmware of the sensor patch. Processing the detected bio-signals within the E-skin patch and wirelessly transmitting fewer data points that contain the necessary key information can reduce the power consumption for wireless data transmission and also the amount of data for post-processing. The block diagram for detecting the R peak of the measured ECG analog signal and wireless transmission of the R peak data using the sensor system is presented in **Figure 7**a. Examples of the resultant signals after performing each step shown in the block diagram are presented in Figure 7b.

To confirm the on-body operation of the developed algorithm, the measured ECG signals were also wirelessly transmitted. In Figure 7c, the wireless readout points of the detected R peaks (indicated as red-colored inverted triangles) and the corresponding continuous wireless readouts of ECG signals obtained during the human trials are presented. The wireless readout of R points well matched the R peak data of the continuous ECG signals. Heart rate and respiration rate (RR) were also estimated using the wireless readout of R points. The heart rate ranged between 68 and 77 beats per minute (bpm) and the RR was approximately 14 breaths per minute. The facile addition of functionality of the hybrid E-skin patch would further enable a health-condition adaptive operation of the sensor patch when combined with other types of sensor systems for more personalized digital healthcare and energy-efficient health monitoring.

3. Conclusion

We have developed a facile approach to enable the great skin comfort of a versatile hybrid E-skin patch containing non-stretchable, stiff components and circuits. A Kagome-based metastructure of breathable, stretchable biomedical adhesive was demonstrated as a skin comfortable platform material of the hybrid E-skin patch through both simulations and human trials. An FPCB-based all-in-one wireless ECG sensor system was tethered to the skin via the Kagome metastructure and was successfully worn for five days without causing significant skin discomfort. Wireless transmission of R peaks of ECG signals for monitoring of heart rates and respiration rates using fewer data points and thus lower energy consumption was also demonstrated. We envision that our facile and versatile strategy could extend the types of materials and devices and significantly simplify the processes to fabricate emerging on-skin electronics and biomedical devices with additional functionality in the fields of digital healthcare, preventive medicine, neuroengineering, human-machine interfaces, and smart prosthetics.

4. Experimental Section

DIC Analysis: The strain induced on the skin under normal motions was investigated using digital image correlation (DIC), a non-contact-type full-field strain measurement method.[43] Commercial software VIC-snap and VIC-3D (Correlated Solutions) were used for collecting and analyzing the full-field data. The study was performed based on the regulations of the Institutional Review Board (IRB) of Seoul National University (SNU, IRB#: 2007/003-040). The volunteer subjects were

© 2022 The Authors. Advanced Materials Technologies published by Wiley-VCH GmbH

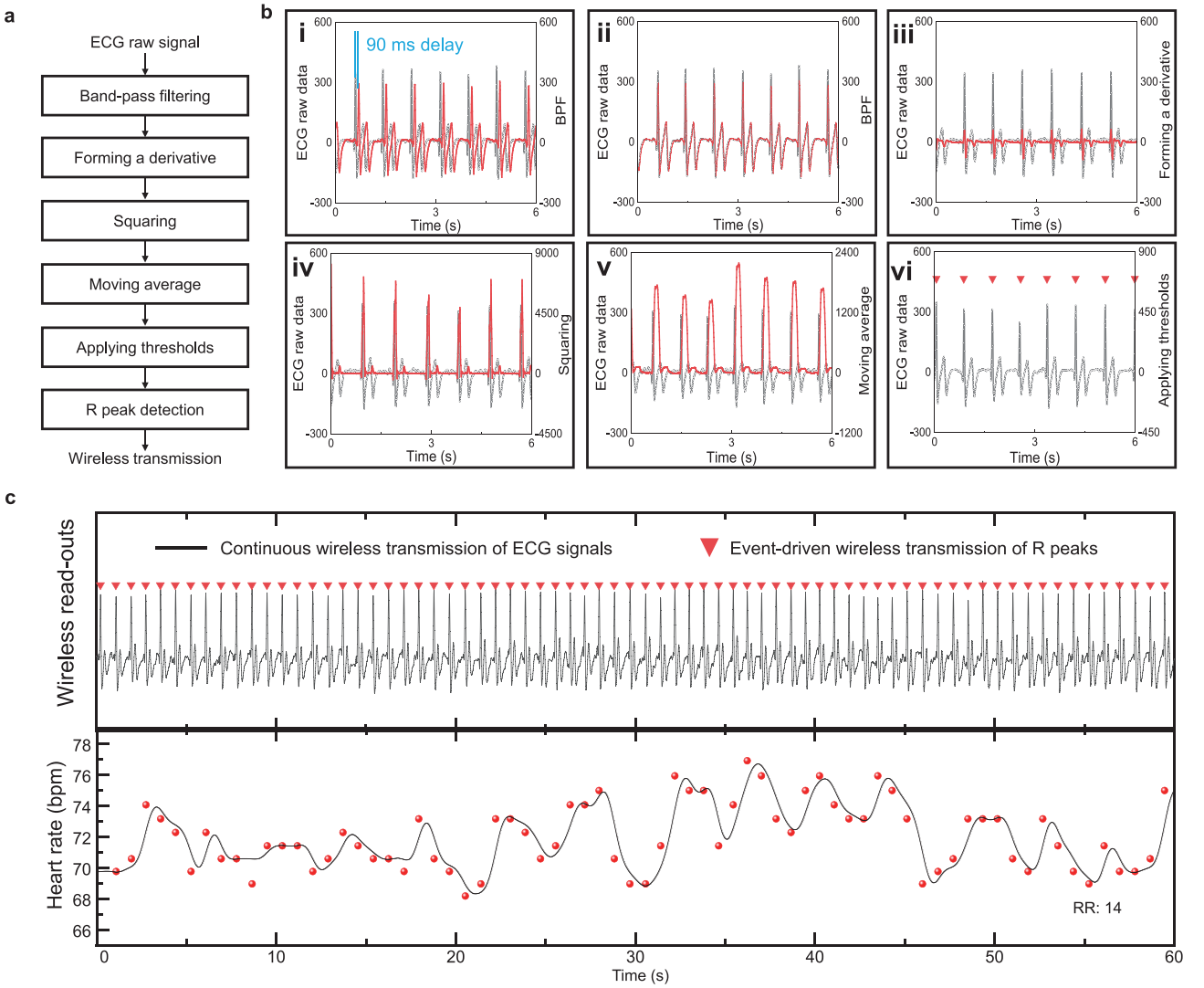

Figure 7. Facile addition of functionality of the hybrid E-skin patch. a) Algorithm developed to detect the R peaks of ECG curves for wireless transmission of measured signals with a reduced amount of data that is nevertheless sufficient to provide necessary information such as heart rate and respiration rate. b) Digital signal processing for the real-time R peak detection within the sensor patch. Grey curves show the raw ECG signals and the red curves and symbols show the resultant signals after performing each step. A delay of about 90 ms occurred due to data processing. As a result of the delay, a data buffer was used to shift the raw data. For the real-time R peak detection, the processing included i-ii) Band-pass filtering (BPF), iii) Forming a derivative, iv) Squaring, v) Moving average, and vi) Applying thresholds for the detection of R peaks. c) Top: wireless readouts of the ECG signal and R peak data. Bottom: the calculated heart rates (red dots) from the wireless readout of the R peak shown in the top panel. The solid line shows a fit to the heart rate data and forms a wave corresponding to respiration activity. A respiration rate (RR) of 14 breaths per minute was obtained from this line.

informed of the risks and benefits of their participation in this study and agreed to participating based on this information. The dimensions of the target area were 100 mm × 120 mm at the chest, considering the ECG patch size (Supplimentary Figure S16). Due to possible differences between the subjects, the measurements were taken for three participants and repeated three times for each participant; then averaged values were used.

FEM Analysis: A finite element simulation was conducted using ABAQUS/standard to calculate the strain levels induced on the skin and the sensor patch as a result of stretching the patch-attached skin. Material properties of the Ecoflex spacer and Tegaderm were determined by performing uniaxial tensile tests (Supplementary Figure S5), and those of the skin were determined as described in the Supplementary Methods and Figure S6–S7. Detailed information about the simulation set-ups is presented in the supplementary Methods.

Trials with Human Participants for the Comparison of Skin Discomfort Resulting from the Use of Various Mechanical Metamaterials: The experiment was carried out with the approval of the IRB of Seoul National University (SNU, IRB#: 2104/003-001), and the data were collected from twenty-six participants and were subjected to statistical analysis. In the experiment, each patch was attached to a position where the signal could be measured. The subjects were directed to perform Motion 1 and Motion 2 as illustrated in Figure 2a and 3b (Motion images were created using a Magic Poser application (Wombat Studio, Inc.)) and to express the extent of the discomfort as a number between 0 and 10 (0: no feeling of anything attached, 10: the feeling when Motion 1 was performed with the rectangular (control) patch attached). Based on ANOVA analysis and subsequent F-test analysis of the results of repeatedly collected data for the same group, the mean difference between the groups were compared with the mean values.

© 2022 The Authors. Advanced Materials Technologies published by Wiley-VCH GmbH

Fabrication of the Sensor System for the Kagome Metastructure-Tethered Hybrid Wireless ECG Sensor Patch: The design of the FPCB of the sensor system was determined by considering the Kagome metastructure as depicted in Figure 1a. A two-layered FPCB composed of a copper/PI/copper thin film (each with a thickness of 25 µm) with patterned cover layers (13-µm-thick PI and 25-µm-thick adhesive) was used for the fabrication of the sensor system (Supplementary Figure S11). The exposed copper layer was plated with electroless nickel immersion gold (3.5-µm-thick layer of Ni, and 0.03-µm-thick layer of Au) to form the dry ECG electrode and also the soldering pads for mounting components. The width of the copper interconnection between the electrode and the sensor system was 100 µm. Solder cream (LF999, KELLYSHUN) and wire (XL806, Alpha Assembly Solutions) were used to solder the components including an AFE IC (AD8232, Analog Devices), linear regulator (AP2112K, Diodes Incorporated), wireless communication microcontroller (nRF52832, Nordic Semiconductor) and various passive elements. The analog output signal of the AFE IC was transmitted as data through a smartphone app (nRFconnect, Nordic Semiconductor) using ADC and BLE communication installed in the microcontroller. A lithium polymer battery was connected to the sensor system for taking the measurements. By implementing the R peak detection algorithm in the firmware used, the raw ECG signal data and the R peak data were processed simultaneously.

Fabrication of the Kagome Metastructure-Tethered Hybrid Wireless ECG Sensor Patch: A programmable cutter (Explore Air 2, Cricut, Inc.) was used to cut a piece of the biomedical adhesive, Tegaderm (3M), into the desired patterns as shown in Figure 1a. A ring-shaped elastomeric spacer was fabricated by curing Ecoflex 00–30 (Smooth-On. Inc.) with a mixing ratio of 1:1 at room temperature. The bottom side of the FPCB-based sensor system was attached to the adherent surface of the bottom Tegaderm layer and then Ecoflex spacers were placed on the ring-shaped dry electrodes of the sensor system. Then, the sensor system was attached to the adherent surface of the top Tegaderm layer. The assembled hybrid sensor patch was then attached to the skin. Information on the durability of the sensor patch can be found in Supplementary Figure S17.

On-Body Evaluations of the Kagome Metastructure-Tethered Hybrid Wireless ECG Sensor Patch: The experimental protocol for taking measurements on the bodies of human participants was approved by the IRB (IRB# 2020–028, 2021–034, 2022-006) of the Korea Institute of Science and Technology. Participants were informed of the risks and benefits of the measurements and consented to having these measurements taken. For the continuous on-body evaluations, the hybrid sensor patch to which a battery was connected was attached to the chest skin of the participant for longer than 20 h and the signals were collected for 2 minutes every hour using a smartphone via BLE. To test the long-term stability of the functioning of the hybrid sensor patch and to determine how comfortable on the skin the patch would be when worn for a long time, the patch was worn for five days and ECG signals were measured for 2 minutes at 2 PM every day using a smartphone.

Characterizations: The surface morphology of the dry sensing electrode was examined by the scanning electron microscopy (Teneo VS, FEI).The SNR was calculated using the equation, $SNR\ (dB) = 20\ \mathrm{Log}_{10}(A_{QRS}/A_{noise})$ and the amplitude of the QRS and the highest noise were obtained using the FFT spectra of the measured ECG curves in the frequency range of 5~15 Hz[48,49] and >15 Hz, respectively.

Supporting Information

Supporting Information is available from the Wiley Online Library or from the author.

Acknowledgements

W.H. and J.K. contributed equally to this work. This work was supported by the Samsung Research Funding Center of Samsung Electronics under Project No. SRFC-TA1803-03. This work was also supported by the National Research Foundation of Korea (NRF) (Nos. 2021R1A2C3011450 and 2019R1A2C2003430).

Conflict of Interest

The authors declare the following competing financial interest: Korea Institute of Science and Technology and Seoul National University R&DB Foundation have filed a patent related to this work (application no. 10-2021-0102651 (KR) and application no. 17/511,576 (US)).

Data Availability Statement

The data that support the findings of this study are available in the supplementary material of this article.

Keywords

breathable electronic skin, digital healthcare, hybrid electronic skin patch, mechanical metastructure, wireless sensor system

Received: March 23, 2022
Revised: July 8, 2022
Published online:

[1] D. Kim, N. Lu, R. Ma, Y. Kim, R. Kim, S. M. Wang, J. Wu, S. M. Won, H. Tao, A. Islam, K. J. Yu, T. I. Kim, R. Chowdhury, M. Ying, L. Xu, M. Li, H. J. Chung, H. Keum, M. McCormick, P. Liu, Y. W. Zhang, F. G. Omenetto, Y. Huang, T. Coleman, J. A. Rogers, *Science* **2011**, *333*, 838.
[2] D. H. Kim, R. Ghaffari, N. S. Lu, J. A. Rogers, *Annu. Rev. Biomed. Eng.* **2012**, *14*, 113.
[3] I. You, B. Kim, J. Park, K. Koh, S. Shin, S. Jung, U. Jeong, *Adv. Mater.* **2016**, *28*, 6359.
[4] B. Wang, A. Facchetti, *Adv. Mater.* **2019**, *31*, 1901408.
[5] C. Wang, K. Xia, M. Zhang, M. Jian, Y. Zhang, *ACS Appl. Mater. Interfaces* **2017**, *9*, 39484.
[6] H. U. Chung, B. H. Kim, J. Y. Lee, J. Lee, Z. Xie, E. M. Ibler, K. Lee, A. Banks, J. Y. Jeong, J. Kim, C. Ogle, D. Grande, Y. Yu, H. Jang, P. Assem, D. Ryu, J. W. Kwak, M. Namkoong, J. B. Park, Y. Lee, D. H. Kim, A. Ryu, J. Jeong, K. You, B. Ji, Z. Liu, Q. Huo, X. Feng, Y. Deng, Y. Xu, et al., *Science* **2019**, *363*, eaau0780.
[7] Y. Ma, Y. Zhang, S. Cai, Z. Han, X. Liu, F. Wang, Y. Cao, Z. Wang, H. Li, Y. Chen, X. Feng, *Adv. Mater.* **2020**, *32*, 1902062.
[8] T. H. Kang, H. Chang, D. Choi, S. Kim, J. Moon, J. A. Lim, K. Y. Lee, H. Yi, *Nano Lett.*. **2019**, *19*, 3684.
[9] K. Takei, W. Gao, C. Wang, A. Javey, *Proc. IEEE* **2019**, *107*, 2155.
[10] E. Song, J. Li, S. M. Won, W. Bai, J. A. Rogers, *Nat. Mater.* **2020**, *19*, 590.
[11] Y. Yu, J. Nassar, C. Xu, J. Min, Y. Yang, A. Dai, R. Doshi, A. Huang, Y. Song, R. Gehlhar, A. D. Ames, W. Gao, *Sci. Robot.* **2020**, *5*, eaaz7946.
[12] H. Chang, S. Kim, S. Jin, S. W. Lee, G. T. Yang, K. Y. Lee, H. Yi, *ACS Appl. Mater. Interfaces* **2018**, *10*, 1067.
[13] Y. Wu, Y. Liu, Y. Zhou, Q. Man, C. Hu, W. Asghar, F. Li, Z. Yu, J. Shang, G. Liu, M. Liao, R. W. Li, *Sci. Robot.* **2018**, *3*, eaat0429.
[14] P. Jiang, J. Winkley, C. Zhao, R. Munnoch, G. Min, L. T. Yang, *IEEE Syst. J.* **2016**, *10*, 1147.
[15] K. H. Yu, A. L. Beam, I. S. Kohane, *Nat. Biomed. Eng.* **2018**, *2*, 719.
[16] C. Wang, C. Pan, Z. Wang, *ACS Nano* **2019**, *13*, 12287.

© 2022 The Authors. Advanced Materials Technologies published by Wiley-VCH GmbH

[17] N. Yi, Y. Gao, A. Lo Verso Jr., J. Zhu, D. Erdely, C. Xue, R. Lavelle, H. Cheng, *Mater. Today* **2021**, *50*, 24.
[18] L. Zhang, H. Ji, H. Huang, N. Yi, X. Shi, S. Xie, Y. Li, Z. Ye, P. Feng, T. Lin, X. Liu, X. Leng, M. Li, J. Zhang, X. Ma, P. He, W. Zhao, H. Cheng, *ACS Appl. Mater. Interfaces* **2020**, *12*, 45504.
[19] Y. Lee, J. W. Chung, G. H. Lee, H. Kang, J. Y. Kim, C. Bae, H. Yoo, S. Jeong, H. Cho, S. G. Kang, J. Y. Jung, D. W. Lee, S. Gam, S. G. Hahm, Y. Kuzumoto, S. J. Kim, Z. N. Bao, Y. Hong, Y. Yun, S. Kim, *Sci. Adv.* **2021**, *7*, eabg9180.
[20] C. Zhang, H. Chen, X. Ding, F. Lorestani, C. Huang, B. Zhang, B. Zheng, J. Wang, H. Cheng, Y. Xu, *Appl. Phys. Rev.* **2022**, *9*, 011413.
[21] H. J. Kil, S. R. Kim, J. W. Park, *ACS. Appl. Mater. Inter.* **2022**, *14*, 3838.
[22] Y. S. Kim, M. Mahmood, Y. Lee, N. K. Kim, S. Kwon, R. Herbert, D. Kim, H. C. Cho, W. H. Yeo, *Adv. Sci.* **2019**, *6*, 1900939.
[23] K. Bertoldi, V. Vitelli, J. Christensen, M. van Hecke, *Nat. Rev. Mater.* **2017**, *2*, 17066.
[24] X. Ren, R. Das, P. Tran, T. D. Ngo, Y. M. Xie, *Smart Mater. Struct.* **2018**, *27*, 023001.
[25] Y. Cho, J. H. Shin, A. Costa, T. A. Kim, V. Kunin, J. Li, S. Y. Lee, S. Yang, H. N. Han, I. S. Choi, D. J. Srolovitz, *Proc. Natl. Acad. Sci. USA* **2014**, *111*, 17390.
[26] K. B. Kim, Y. J. Lee, A. Costa, Y. K. Lee, T. S. Jang, M. G. Lee, Y. C. Joo, K. H. Oh, J. Song, I. S. Choi, *Adv. Eng. Mater.* **2019**, *21*, 1900206.
[27] Y. J. Lee, S. M. Lim, S. M. Yi, J. H. Lee, S. G. Kang, G. M. Choi, H. N. Han, J. Y. Sun, I. S. Choi, Y. C. Joo, *Extreme. Mech. Lett.* **2019**, *31*, 100516.
[28] H. Yeon, H. Lee, Y. Kim, D. Lee, Y. Lee, J. S. Lee, J. Shin, C. Choi, J. H. Kang, J. M. Suh, H. Kim, H. S. Kum, J. Lee, D. Kim, K. Ko, B. S. Ma, P. Lin, S. Han, S. Kim, S. H. Bae, T. S. Kim, M. C. Park, Y. C. Joo, E. Kim, J. Han, J. Kim, *Sci. Adv.* **2021**, *7*, eabg8459.
[29] Y. Jiang, Z. Liu, N. Matsuhisa, D. Qi, W. Leow, H. Yang, J. Yu, G. Chen, Y. Liu, C. Wan, Z. Liu, X. Chen, *Adv. Mater.* **2018**, *30*, 1706589.
[30] S. Han, S. Jung, S. Jeong, J. Choi, Y. Choi, S. Y. Lee, *J. Mater. Chem. C* **2020**, *8*, 1556.
[31] J. Liu, D. Yan, Y. Zhang, *J. Mech. Phys. Solids.* **2021**, *146*, 104210.
[32] D. Yan, J. Chang, H. Zhang, J. Liu, H. Song, Z. Xue, F. Zhang, Y. Zhang, *Nat. Commun.* **2020**, *11*, 1180.
[33] Y. Yu, H. Yuk, G. A. Parada, Y. Wu, X. Y. Liu, C. S. Nabzdyk, K. Youcef-Toumi, J. F. Zang, X. H. Zhao, *Adv. Mater.* **2019**, *31*, 1807101.
[34] Q. Ma, H. Y. Cheng, K. I. Jang, H. W. Luan, K. C. Hwang, J. A. Rogers, Y. G. Huang, Y. H. Zhang, *J. Mech. Phys. Solids* **2016**, *90*, 179.
[35] K. I. Jang, H. U. Chung, S. Xu, C. H. Lee, H. W. Luan, J. Jeong, H. Y. Cheng, G. T. Kim, S. Y. Han, J. W. Lee, J. Kim, M. Cho, F. X. Miao, Y. Y. Yang, H. N. Jung, M. Flavin, H. Liu, G. W. Kong, K. J. Yu, S. I. Rhee, J. Chung, B. Kim, J. W. Kwak, M. H. Yun, J. Y. Kim, Y. M. Song, U. Paik, Y. H. Zhang, Y. Huang, J. A. Rogers, *Nat. Commun.* **2015**, *6*, 6566.
[36] H. W. Kim, T. Y. Kim, H. K. Park, I. You, J. Kwak, J. C. Kim, H. Hwang, H. S. Kim, U. Jeong, *ACS Appl. Mater. Interfaces* **2018**, *10*, 40141.
[37] T. H. Park, S. Park, S. Yu, S. Park, J. Lee, S. Kim, Y. Jung, H. Yi, *Adv. Healthcare Mater.* **2021**, *10*, 2100469.
[38] J. Choi, R. Ghaffari, L. B. Baker, J. A. Rogers, *Sci. Adv.* **2018**, *4*, eaar3921.
[39] A. Miyamoto, S. Lee, N. F. Cooray, S. Lee, M. Mori, N. Matsuhisa, H. Jin, L. Yoda, T. Yokota, A. Itoh, M. Sekino, H. Kawasaki, T. Ebihara, M. Amagai, T. Someya, *Nat. Nanotechnol.* **2017**, *12*, 907.
[40] B. H. Sun, R. N. McCay, S. Goswami, Y. D. Xu, C. Zhang, Y. Ling, J. Lin, Z. Yan, *Adv. Mater.* **2018**, *30*, 1804327.
[41] W. X. Zhou, S. S. Yao, H. Y. Wang, Q. C. Du, Y. W. Ma, Y. Zhu, *ACS Nano* **2020**, *14*, 5798.
[42] J. I. Ngadaonye, L. M. Geever, K. E. McEvoy, J. Killion, D. B. Brady, C. L. Higginbotham, *Int. J. Polym. Mater. Polym. Biomater.* **2014**, *63*, 873.
[43] T. C. Chu, W. F. Ranson, M. A. Sutton, W. H. Peters, *Exp. Mech.* **1985**, *25*, 232.
[44] H. Joodaki, M. B. Panzer, *P. I. Mech. Eng. H* **2018**, *232*, 323.
[45] S. L. Evans, C. A. Holt, *J. Strain. Anal. Eng.* **2009**, *44*, 337.
[46] E. L. Plan, J. P. Elshoff, A. Stockis, M. L. Sargentini-Maier, M. O. Karlsson, *Clin. Pharmacol. Ther.* **2012**, *91*, 820.
[47] C. M. Hicks, R. Gonzales, M. T. Morton, R. V. Gibbons, R. S. Wigton, R. J. Anderson, *J. Gen. Intern. Med.* **2000**, *15*, 716.
[48] N. V. Thakor, J. G. Webster, W. J. Tompkins, *Med. Biol. Eng. Comput.* **1983**, *21*, 343.
[49] H. C. Chen, S. W. Chen, *Comput. Cardiol.* **2003**, *30*, 585.
[50] X. Xu, T. Yang, Y. Yu, W. Xu, Y. Ding, H. Hou, *J. Mater. Sci. Mater. Electron.* **2017**, *28*, 12683.
[51] S. D. Zhang, M. Sakane, T. Nagasawa, K. Kobayashi, *Proc. Eng.* **2011**, *10*, 1497.
[52] N. S. Lu, Z. G. Suo, J. J. Vlassak, *Acta Mater.* **2010**, *58*, 1679.
[53] M. Sugiyama, T. Uemura, M. Kondo, M. Akiyama, N. Namba, S. Yoshimoto, Y. Noda, T. Araki, T. Sekitani, *Nat. Electron.* **2019**, *2*, 351.
[54] H. Lee, S. Lee, W. Lee, T. Yokota, K. Fukuda, T. Someya, *Adv. Funct. Mater.* **2019**, *29*, 1906982.

© 2022 The Authors. Advanced Materials Technologies published by Wiley-VCH GmbH